

Polarization dynamics in a photon Bose-Einstein Condensate

Ryan I. Moodie, Peter Kirton, and Jonathan Keeling

SUPA, School of Physics and Astronomy, University of St Andrews, St Andrews, KY16 9SS, United Kingdom

(Dated: November 20, 2021)

It has previously been shown that a dye-filled microcavity can produce a Bose-Einstein condensate of photons. Thermalization of photons is possible via repeated absorption and re-emission by the dye molecules. In this paper, we theoretically explore the behavior of the polarization of light in this system. We find that in contrast to the near complete thermalization between different spatial modes of light, thermalization of polarization states is expected to generally be incomplete. We show that the polarization degree changes significantly from below to above threshold, and explain the dependence of polarization on all relevant material parameters.

I. INTRODUCTION

By trapping photons in a high quality multimode resonator, and allowing them to interact with emitters such as dye molecules, it is possible to form a thermalized gas of photons, and at high enough densities, a Bose-Einstein condensate [1, 2]. The crucial feature in these experiments is the complex spectrum of typical dye molecules: there are broad absorption and emission spectra, and these spectra are related to each other by a Boltzmann factor (a feature known as the Kennard-Stepanov relation [3–5]). This behavior arises because the internal rovibrational state of the molecules rapidly reaches thermal equilibrium due to collisions between dye molecules and the solvent. In turn, this Boltzmann factor between emission and absorption leads to a Bose-Einstein distribution of the photon energy, as long as they can be absorbed and re-emitted many times before escaping the cavity.

The observation of Bose-Einstein condensation of photons has led to many subsequent theoretical discussions and experimental extensions [6–27], based in part on the simplicity of the material system. Here we focus on an aspect that has only recently been cursorily studied [28, 29], the dynamics of polarization.

Polarization dynamics has of course been extensively studied for other Bose-Einstein condensates, for a variety of reasons. In ultracold atoms, a number of questions have been studied [30, 31] such as the dynamics following a sudden quench, leading to the formation of domains, and non-trivial coarsening dynamics — for a review of these topics, see e.g. Stamper-Kurn and Ueda [32]. In Helium, there can be a complex spinor structure arising from spin-orbit coupling, and this in turn can lead to complex topological defects [33, 34]. Most directly relevant to the photon BEC system is the study of polarization dynamics in polariton condensates, which has been reviewed by Shelykh *et al.* [35].

For both photon and polariton condensates, the polarization state of a condensate can serve as a clear test of the relative roles of energetics vs the balance of pumping and decay. Were the system to fully reach equilibrium, the polarization state would be entirely determined by any energetic splitting between polarized states. Exper-

iments on polaritons [36] have however seen cases where the higher energy of two Zeeman split states becomes macroscopically occupied. Such observations are often clearer than the equivalent behavior in terms of competition between different spatial modes: the polarization state can be described by a small number of parameters, and so fully quantified. However, in polariton systems this is complicated by an intrinsic splitting between different linear polarization states which arises from the quantum well structure [37, 38]. Nonetheless, theoretical models have been developed [39, 40] that compare well to experiments.

In this paper, we develop a model for the polarization dynamics of a dye-filled microcavity. We show that in contrast to the spatial dynamics, which is expected to fully thermalize in the limit of a perfect cavity [22], the polarization state need not do so. This means that the output polarization depends on the polarization of the pump light. This dependence varies significantly from below to above threshold. Below threshold, rotational diffusion of molecules destroys polarization, while above threshold, stimulated emission overcomes this, leading to a highly polarized state. The model we develop accounts for specific dynamics of the photon condensate, namely the repeated absorption and re-emission of light by dye molecules. This requires developing coupled equations for the polarization state of the light in the cavity, as well as for the state of the dye molecules. Such a model is thus quite different from the typical situations encountered in e.g. atomic condensates [30, 31].

Our paper is organized as follows. Section II introduces the model we consider, and provides a discussion of the parameters which appear. We then use this model in Section III to explore the dependence on various parameters. First, to orient the reader, we illustrate typical states found below and above threshold (i.e. showing the occupations of all spatial and polarization modes). We then proceed to extract a net polarization of the output, and explore the dependence of this characteristic quantity upon all relevant parameters. Finally, in Section IV we summarize our results.

II. MODEL

A. Underpinning Hamiltonian

Our basic starting point is a modified form of the multimode Jaynes-Cummings model

$$\hat{H} = \sum_{\mathbf{m}} \omega_{\mathbf{m}} \hat{a}_{\mathbf{m}}^{\dagger} \hat{a}_{\mathbf{m}} + \sum_i \epsilon \sigma_i^+ \sigma_i^- + g \sum_{\mathbf{m}, i} (\hat{a}_{\mathbf{m}} \hat{\sigma}_i^+ + \hat{a}_{\mathbf{m}}^{\dagger} \hat{\sigma}_i^-) + H_{\text{rovibrational}} \quad (1)$$

using units such that $\hbar = 1$. As discussed previously [9, 16], the thermalization of photons by dye fluorescence can be modeled by considering how the electronic transitions of a molecule are dressed by coupling to internal vibrational degrees of freedom of the molecule. After a polaron transform, these degrees of freedom appear as dressing the electronic transitions, by the replacement $\sigma_i^+ \rightarrow \sigma_i^+ \hat{D}_i$ where $\hat{D}_i = \exp \left[\sum_{\alpha} \sqrt{S_{\alpha}} (\hat{b}_{\alpha, i}^{\dagger} - \hat{b}_{\alpha, i}) \right]$ with $\hat{b}_{\alpha, i}$ the annihilation operator for the α th rovibrational mode of molecule i , and $\sqrt{S_{\alpha}}$ the corresponding Huang-Rhys parameter. In the weak coupling limit, the matter-light coupling can be treated perturbatively, leading to incoherent emission and absorption processes, described in a master equation by terms

$$\dot{\rho} = \dots + \sum_{\mathbf{m}, i} \Gamma(-\delta_{\mathbf{m}} = \epsilon - \omega_{\mathbf{m}}) \mathcal{L}[\hat{a}_{\mathbf{m}}^{\dagger} \sigma_i^-, \rho] + \Gamma(\delta_{\mathbf{m}} = \omega_{\mathbf{m}} - \epsilon) \mathcal{L}[\hat{a}_{\mathbf{m}} \sigma_i^+, \rho]. \quad (2)$$

Here the function $\Gamma(\delta)$ can be calculated from the Fourier transform of the two-time correlation function of the operators $\hat{D}_i(t)$ and $\hat{D}_i^{\dagger}(t')$. Further details are given in Ref. [16]. Crucially, for thermalized vibrational degrees of freedom one finds the Kennard-Stepanov [3–5] relation $\Gamma(-\delta) = e^{-\beta\delta} \Gamma(\delta)$. Alternatively, the function $\Gamma(\delta)$ can be found experimentally from the observed fluorescence of the dye. We will use this approach, and specifically the spectrum extracted from experimental measurement of Rhodamine 6G [41], as in Ref. [22] here.

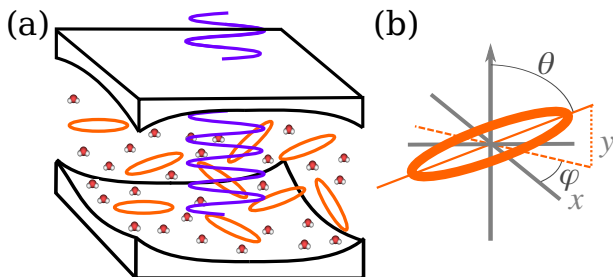


FIG. 1. (a) Cartoon illustrating the physical system we consider, and (b) the angles defining the orientation of a molecule. Orange ellipses represent dye molecules, indicating the principal axes of the electric dipole, sitting in a background of solvent molecules. A fully y polarized pump is shown in (a).

To consider the polarization state of the light there are two changes we must make. We must obviously keep track separately of the different polarization components of the light, and we must also take account of the orientation of the dipole moments of the molecules. We consider a limit where the molecules are strongly anisotropic, so there is only a single non-degenerate electronic excited state that is relevant, and a single associated dipole moment for the ground to excited state transition. (For a situation where the molecule is more spherically symmetric, would require one to keep track of multiple electronic excited states, and the orientation of the dipole moment for transitions to each state separately.) Accounting for polarization leads to a modified Hamiltonian, of the form

$$\hat{H} = \sum_{\mathbf{m}, \sigma=x, y} \omega_{\mathbf{m}} \hat{a}_{\sigma \mathbf{m}}^{\dagger} \hat{a}_{\sigma \mathbf{m}} + \sum_i \epsilon \sigma_i^+ \sigma_i^- + g \sum_{\mathbf{m}, \sigma, i} \hat{\mathbf{e}}_{\sigma} \cdot \hat{\mathbf{d}}_i (\hat{a}_{\sigma \mathbf{m}} \hat{\sigma}_i^+ + \hat{a}_{\sigma \mathbf{m}}^{\dagger} \hat{\sigma}_i^-). \quad (3)$$

In comparison to Eq. (1), the crucial extra feature in Eq. (3) is that we take account of the orientation $\hat{\mathbf{d}}_i$ of the dipole moment of molecule i , and how this affects its coupling to light with polarization $\hat{\mathbf{e}}_{\sigma=x, y} = \hat{\mathbf{x}}, \hat{\mathbf{y}}$. As illustrated in Fig. 1, the orientation of molecule i can be parameterized by the polar angles θ_i, ϕ_i describing the orientation with respect to the cavity axis, and yields $\hat{\mathbf{e}}_{\sigma=x, y} \cdot \hat{\mathbf{d}}_i = \sin \theta_i \times (\cos \phi_i, \sin \phi_i)$ respectively. The intra-molecular coupling between the electronic state and vibrational state of a given molecule is not dependent on how the molecule is oriented with respect to any external axis, and so its treatment remains the same as our earlier model that ignored polarization. In addition to these incoherent processes considered previously, we will also add one extra crucial process: rotational diffusion of the molecules. This means we will assume the orientation of each molecule varies randomly. If this process is fast, the fluorescence of the molecules is unpolarized even for a polarized pump, as the orientation of molecules when they emit and when they absorb becomes uncorrelated.

The model we consider neglects any direct interactions between different dye molecules. i.e., there is no Förster resonance energy transfer process between molecules. Such an assumption is reasonable for current experiments, where the dye concentrations mean the typical distance between molecules exceeds 10nm, but may play a rôle in experiments with other materials or at higher concentrations.

B. Equations of motion in angle space

Rather than considering the full (and computationally intractable) dynamics of the photon and molecule density matrix, we follow the same approach as used previously [9, 16] and consider a semiclassical analysis. Neglecting polarization, the state of the system is described by two types of quantity: the population

$n_{\mathbf{m}} = \langle \hat{a}_{\mathbf{m}}^\dagger \hat{a}_{\mathbf{m}} \rangle$ of photons in a given mode, \mathbf{m} , and the number $N_{\uparrow} = \sum_i \langle \sigma_i^+ \sigma_i^- \rangle$ of molecules in the excited state. When we account for the polarization of light, and its selective coupling to molecules with dipole moments oriented in a given direction, both of these become more complicated. For light we must now consider the

co- and cross-polarization components $n_{\mathbf{m}}^{\sigma\sigma'} = \langle \hat{a}_{\sigma\mathbf{m}}^\dagger \hat{a}_{\sigma'\mathbf{m}} \rangle$, while for molecules we have to consider not only the total population, but its angular distribution $N_{\uparrow}(\theta, \phi) = \sum_i \delta(\theta - \theta_i) \delta(\phi - \phi_i) \langle \sigma_i^+ \sigma_i^- \rangle$, which in the large N limit can be considered as a continuous function.

Taking into account all the processes described above, the equations of motion for the populations and coherences of the cavity modes take the form:

$$\begin{aligned} \frac{\partial}{\partial t} n_{\mathbf{m}}^{xx} = -\kappa n_{\mathbf{m}}^{xx} + \iint d\Omega \sin^2(\theta) \left\{ \Gamma(-\delta_{\mathbf{m}}) \left[\cos^2(\phi)(n_{\mathbf{m}}^{xx} + 1) + \frac{1}{2} \sin(\phi) \cos(\phi) (n_{\mathbf{m}}^{xy} + \overline{n_{\mathbf{m}}^{xy}}) \right] N_{\uparrow}(\theta, \phi) \right. \\ \left. - \Gamma(\delta_{\mathbf{m}}) \left[\cos^2(\phi) n_{\mathbf{m}}^{xx} + \frac{1}{2} \sin(\phi) \cos(\phi) (n_{\mathbf{m}}^{xy} + \overline{n_{\mathbf{m}}^{xy}}) \right] (N - N_{\uparrow}(\theta, \phi)) \right\} \quad (4) \end{aligned}$$

$$\begin{aligned} \frac{\partial}{\partial t} n_{\mathbf{m}}^{yy} = -\kappa n_{\mathbf{m}}^{yy} + \iint d\Omega \sin^2(\theta) \left\{ \Gamma(-\delta_{\mathbf{m}}) \left[\sin^2(\phi)(n_{\mathbf{m}}^{yy} + 1) + \frac{1}{2} \sin(\phi) \cos(\phi) (n_{\mathbf{m}}^{xy} + \overline{n_{\mathbf{m}}^{xy}}) \right] N_{\uparrow}(\theta, \phi) \right. \\ \left. - \Gamma(\delta_{\mathbf{m}}) \left[\sin^2(\phi) n_{\mathbf{m}}^{yy} + \frac{1}{2} \sin(\phi) \cos(\phi) (n_{\mathbf{m}}^{xy} + \overline{n_{\mathbf{m}}^{xy}}) \right] (N - N_{\uparrow}(\theta, \phi)) \right\} \quad (5) \end{aligned}$$

$$\begin{aligned} \frac{\partial}{\partial t} n_{\mathbf{m}}^{xy} = -\kappa n_{\mathbf{m}}^{xy} + \frac{1}{2} \iint d\Omega \sin^2(\theta) \left\{ \Gamma(-\delta_{\mathbf{m}}) \left[n_{\mathbf{m}}^{xy} + \sin(\phi) \cos(\phi) (n_{\mathbf{m}}^{xx} + n_{\mathbf{m}}^{yy} + 2) \right] N_{\uparrow}(\theta, \phi) \right. \\ \left. - \Gamma(\delta_{\mathbf{m}}) \left[n_{\mathbf{m}}^{xy} + \sin(\phi) \cos(\phi) (n_{\mathbf{m}}^{xx} + n_{\mathbf{m}}^{yy}) \right] (N - N_{\uparrow}(\theta, \phi)) \right\} \quad (6) \end{aligned}$$

where we have written $\iint d\Omega = \int_0^{2\pi} d\phi \int_0^\pi d\theta \sin(\theta)$ for the integral over solid angles, and the bar indicates complex conjugation. In each of these equations there are two types of processes: simple cavity loss, and emission and absorption from and by the dye molecules. The location of the +1 terms can be understood as arising from the commutator $[\hat{a}_{\mathbf{m}\sigma}, \hat{a}_{\mathbf{m}\sigma'}^\dagger]$.

To complete the description, we need also an equation of motion for the angular distribution of the excited molecules. Note, we are assuming angular diffusion of molecules is independent of the electronic state. This means that the angular distribution of all molecules, $N_{\uparrow}(\theta, \phi) + N_{\downarrow}(\theta, \phi) = N$ is a constant, independent of angle, hence the terms $N - N_{\uparrow}(\theta, \phi)$ appearing above indicate the angular distribution of ground state molecules. Thus, we need only track the evolution of the excited state distribution, $N_{\uparrow}(\theta, \phi)$ which obeys:

$$\begin{aligned} \frac{\partial}{\partial t} N_{\uparrow}(\theta, \phi) = -\Gamma_{\downarrow} N_{\uparrow}(\theta, \phi) + \Gamma_{\uparrow} \sin^2(\theta) \left(\cos^2(\chi) \cos^2(\phi) + \sin^2(\chi) \sin^2(\phi) \right) (N - N_{\uparrow}(\theta, \phi)) \\ + \sum_{\mathbf{m}=0}^{\infty} g_{\mathbf{m}} \sin^2(\theta) \left\{ \Gamma(\delta_{\mathbf{m}}) \left[\cos^2(\phi) n_{\mathbf{m}}^{xx} + \sin^2(\phi) n_{\mathbf{m}}^{yy} + \sin(\phi) \cos(\phi) (n_{\mathbf{m}}^{xy} + \overline{n_{\mathbf{m}}^{xy}}) \right] (N - N_{\uparrow}(\theta, \phi)) \right. \\ \left. - \Gamma(-\delta_{\mathbf{m}}) \left[\cos^2(\phi) (n_{\mathbf{m}}^{xx} + 1) + \sin^2(\phi) (n_{\mathbf{m}}^{yy} + 1) + \sin(\phi) \cos(\phi) (n_{\mathbf{m}}^{xy} + \overline{n_{\mathbf{m}}^{xy}}) \right] N_{\uparrow}(\theta, \phi) \right\} \\ + D \left[\frac{1}{\sin(\theta)} \frac{\partial}{\partial \theta} \left(\sin(\theta) \frac{\partial}{\partial \theta} \right) + \frac{1}{\sin^2(\phi)} \frac{\partial^2}{\partial \phi^2} \right] N_{\uparrow}(\theta, \phi). \quad (7) \end{aligned}$$

where $g_{\mathbf{m}}$ accounts for the degeneracy of a given photon mode energy \mathbf{m} ; in the following we always consider a two-dimensional harmonic oscillator mirror profile, so that $g_{\mathbf{m}} = \mathbf{m} + 1$.

In Eq. (7), the first line represents the external (non-cavity-mediated) loss, and external pumping process acting on the molecules. We consider a pump which has total intensity Γ_{\uparrow} , and a polarization which varies from

fully polarized in the x direction (for $\chi = 0$), through fully unpolarized ($\chi = \pi/4$), to fully polarized in the y direction ($\chi = \pi/2$). In terms of the Bloch sphere of polarization, this means that as χ is varied, one follows an

axis through the center of the sphere. Since pumping of a given molecule depends on the overlap of its dipole moment with the polarization of this pump laser, this leads to the form of the pump term seen. In contrast, the non-cavity-mediated decay (e.g. via non-radiative processes) is assumed independent of the orientation of the molecules. The second and third line of Eq. (7) are the counterpart of the photon rate equations, describing how emission and absorption of cavity light affects the angular distribution of excited molecules. The final line is the rotational diffusion process which we write as a Laplacian with a rate constant D ; these rotational rate constants for a variety of dye molecules in various solvents have been measured in Von Jena and Lessing [42].

Given the form of external pumping we have considered in the equations above, we may note that at late times two interconnected simplifications occur: $n_{\mathbf{m}}^{xy} \rightarrow 0$, and $N_{\uparrow}(\theta, \phi)$ becomes an even function of ϕ . If we consider the second condition first, we note that in Eq. (7), that if $N_{\uparrow}(\theta, \phi)$ is an even function of ϕ , then the only odd terms on the right hand side come from $n_{\mathbf{m}}^{xy}$, with its $\sin(\phi) \cos(\phi) = \sin(2\phi)/2$ dependence. If we then consider Eq. (6), we see that the source term for $n_{\mathbf{m}}^{xy}$ depends precisely on the integral $\iint d\Omega \sin^2(\theta) \sin(2\phi) N_{\uparrow}(\theta, \phi)$. Thus, if $N_{\uparrow}(\theta, \phi)$ is an even function, this source term vanishes. Since diffusion of the molecules causes decay of all angular dependence of $N_{\uparrow}(\theta, \phi)$, and photon loss causes decay of $n_{\mathbf{m}}^{xy}$, we can see that any initial odd harmonics or population of $n_{\mathbf{m}}^{xy}$ will be lost.

The vanishing steady state value of $n_{\mathbf{m}}^{xy}$ is a consequence of our choice of pump polarization: because our pump contains an incoherent mixture of x and y polarized light, it cannot break the phase symmetry for the complex $n_{\mathbf{m}}^{xy}$. If we had chosen alternate axes for the linear polarization components of the pump, then the angular

distribution of excited molecules would have contained odd components, leading to a non-zero values of $n_{\mathbf{m}}^{xy}$. However, such a situation could be reduced to the one we consider by a linear rotation of polarization axes.

One notable consequence of the equations of motion, which we will discuss below, is that even in the absence of diffusion, perfect linear polarization of the pump does not lead to perfect polarization of the cavity light. Microscopically this is because molecules oriented at $\phi = \pi/4$ can couple with $\sin^2 \phi = \cos^2 \phi = 1/2$ to both x and y polarized light. Naively one might have expected that without diffusion, the orthogonal x and y polarizations would decouple. For the molecules to preserve this orthogonality requires inter-molecular coherence. However, due to frequent collisions between the dye molecules and the solvent this coherence vanishes (our equations are written using this assumption) and so the destructive interference does not occur.

C. Equations of motion for angular harmonics

Making use of the above simplification, we have two sets of equations for the photon populations and a partial differential equation for the angle distribution. To solve this numerically, it is helpful to rewrite this distribution in terms of standard spherical harmonics. Specifically we write:

$$N_{\uparrow}(\theta, \phi) = \sum_{l,m} N_{l,m} Y_{l,m}(\theta, \phi),$$

$$Y_{l,m}(\theta, \phi) = \sqrt{\frac{2l+1}{4\pi} \frac{(l-m)!}{(l+m)!}} P_{l,m}(\cos \theta) e^{im\phi}$$

where $P_{l,m}(x)$ are the associated Legendre polynomials.

Written in this way, the photon population equations take a relatively simple form:

$$\frac{\partial}{\partial t} n_{\mathbf{m}}^{xx,yy} = -\kappa n_{\mathbf{m}}^{xx,yy} + \frac{4\pi}{3} \left[\Gamma(-\delta_{\mathbf{m}}) \left\{ (n_{\mathbf{m}}^{xx,yy} + 1) \left[N_{0,0} - \frac{N_{2,0}}{\sqrt{5}} \pm \sqrt{\frac{3}{10}} (N_{2,2} + N_{2,-2}) \right] \right\} \right. \\ \left. - \Gamma(\delta_{\mathbf{m}}) \left\{ n_{\mathbf{m}}^{xx,yy} \left[N - N_{0,0} + \frac{N_{2,0}}{\sqrt{5}} \mp \sqrt{\frac{3}{10}} (N_{2,2} + N_{2,-2}) \right] \right\} \right]. \quad (8)$$

Here, the only difference between the xx and yy populations is the sign of the populations of the $m = \pm 2$ harmonics. One may note that only the even-parity harmonics with $l \in \{0, 2\}$ actually couple to the photon distribution. However, as we will see next, there are (photon induced) couplings between different harmonic components of the molecular distribution.

The equation of motion for $N_{l,m}$ takes a more complicated form, so we introduce various auxiliary quantities $\zeta_{l,m}^{\pm}, \mu_{l,m}^{\pm}$, defined below. In terms of these we have:

$$\frac{\partial}{\partial t} N_{l,m} = -\Gamma_{\downarrow} N_{l,m} + \Gamma_{\uparrow} \left(\cos^2(\chi) \mu_{l,m}^{+} + \sin^2(\chi) \mu_{l,m}^{-} \right) \\ + \sum_{\mathbf{m}=0}^{\infty} g_{\mathbf{m}} \left[\Gamma(\delta_{\mathbf{m}}) \left(n_{\mathbf{m}}^{xx} \mu_{l,m}^{+} + n_{\mathbf{m}}^{yy} \mu_{l,m}^{-} \right) - \Gamma(-\delta_{\mathbf{m}}) \left((n_{\mathbf{m}}^{xx} + 1) \zeta_{l,m}^{+} + (n_{\mathbf{m}}^{yy} + 1) \zeta_{l,m}^{-} \right) \right] - D l(l+1) N_{l,m}. \quad (9)$$

Note here that the label \mathbf{m} denotes cavity modes, while m denotes azimuthal harmonics of the molecular distribution.

The auxiliary quantities are defined by:

$$\mu_{l,m}^{\pm} = \frac{N}{3} \left[\delta_{0,l} \delta_{0,m} - \frac{1}{\sqrt{5}} \delta_{2,l} \delta_{0,m} \pm \sqrt{\frac{3}{10}} (\delta_{2,l} \delta_{2,m} + \delta_{2,l} \delta_{-2,m}) \right] - \zeta_{l,m}^{\pm}, \quad (10)$$

and

$$\begin{aligned} \zeta_{l,m}^{\pm} = \frac{1}{2} \left[\left(1 - \frac{(l-m+1)(l+m+1)}{(2l+1)(2l+3)} - \frac{(l+m)(l-m)}{(2l+1)(2l-1)} \right) N_{l,m} - \sqrt{\frac{(l-m)(l-m-1)(l+m)(l+m-1)}{(2l-3)(2l-1)^2(2l+1)}} N_{l-2,m} \right. \\ \left. - \sqrt{\frac{(l-m+2)(l-m+1)(l+m+2)(l+m+1)}{(2l+1)(2l+3)^2(2l+5)}} N_{l+2,m} \right. \\ \left. \pm \pi \sqrt{\frac{(2l+1)(l-m)!}{4\pi(l+m)!}} \sum_{l'=0}^{\infty} \sum_{m'=m-2, m+2} \sqrt{\frac{(2l'+1)(l'-m')!}{4\pi(l'+m')!}} \int_{-1}^1 dx (1-x^2) P_{l,m}(x) P_{l',m'}(x) N_{l',m'} \right]. \quad (11) \end{aligned}$$

Equations (8)–(11) define the problem that we simulate numerically. From this we can then extract the full spectrum of the photons $n_m^{\sigma\sigma}$, and thus quantities such as the total intensity of x and y polarized light, or the total degree of linear polarization. We truncate the equations at a fixed value of l and, to ensure convergence, we check that all results are insensitive to increasing this cutoff.

D. Parameters

In the following, we show numerical results of these equations, and so must specify parameters. For reference we discuss here the typical parameter values used. Table I provides the values of these parameters. Note that Γ_{\uparrow} is not specified, as we typically scan the pumping strength in order to cross threshold, and we report the ratio $\Gamma_{\uparrow}/\Gamma_{\downarrow}$. The polarization angle of the pump, χ , is always given in all figures (or “full polarization”, i.e. $\chi = 0$ is stated).

Parameter	Meaning	Value
κ	Cavity mode decay rate	0.5 GHz
Γ_{\downarrow}	(Non-cavity) Decay rate of excited electronic state	0.25 GHz
D	Rotational diffusion rate of molecules	0.333 GHz
N	Number of molecules	10^8

TABLE I. Standard parameter values used in figures below unless otherwise specified.

As well as these simple parameters, a crucial parameter choice is the set of values $\Gamma(\delta_m)$ for the different photon modes. We take the same functional form of $\Gamma(\delta)$ as used in Ref. [22], corresponding to the shape of the experimentally measured spectrum of Rhodamine 6G [41], with a peak height around 10 kHz, extracted in Ref. [22] by matching the pump-spot-size dependence of photon cloud below threshold. We then sample at a set of frequencies $\delta_m = \delta_0 + m\epsilon$ where the cavity cutoff frequency is $\delta_0 = 3300$ THz and mode spacing (set by the mirror curvature) of $\epsilon = 2.7$ THz. These parameters mean we are in a regime where the system thermalizes well (i.e. this is significant emission and absorption right down to

the cavity cutoff). It is also important to note that comparing this form of $\Gamma(\delta)$ to the values Γ_{\downarrow} means that at low powers (without stimulated emission), non-cavity loss processes are dominant, leading to a sharp threshold (see Ref. [22] for further details).

III. RESULTS

A. Characteristic steady state mode occupations

Before discussing the dependence of the polarization on external parameters we show the steady state of our equations of motion, plotted in Fig. 2 for two pump powers, one below threshold and the other above threshold. These are plotted for a fully polarized pump, $\chi = 0$, with a non-zero rotational diffusion constant D and other parameters as given in Table I.

In both the below- and above-threshold cases, the distribution closely matches the Bose-Einstein distribution, but above threshold, it is in the regime where a Bose condensed fraction of photons arises. As is clear from the figure, there is a considerable change of the degree of polarization between the below-threshold and above-threshold behavior. This has a simple theoretical explanation: below threshold, the state is almost unpolarized, as the rotational diffusion randomizes the orientation of the molecule between absorption and emission. i.e., the timescale for molecules to rotate is much shorter than the timescale for fluorescence. Thus, despite the polarized pump, the subsequent fluorescence of the molecules produces a nearly unpolarized source of photons in the cavity. Above threshold, the macroscopic population of photons in the low energy mode leads to stimulated emission of photons into that mode. That means the rate of

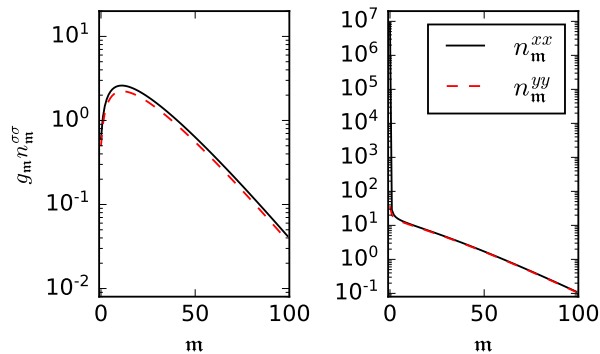


FIG. 2. Occupation of photon states for a fully polarized pump. Left: Below threshold, Right: above threshold. The two lines show the two different polarization states n_m^{xx}, n_m^{yy} . See table I for parameter values.

emission of photons increases, by a factor depending on the occupation of the condensate mode. This increased emission rate means the fluorescence becomes faster than the rotation and so polarization is better preserved. In the following we will systematically explore the dependence of this process on various parameters.

B. Polarization degree across condensation threshold

In order to investigate how the polarization changes from below to above threshold, and to orient further discussion, Fig. 3 summarizes the degree of polarization by first plotting the total light intensity $n_{\text{tot}}^{\sigma=x,y} = \sum_m n_m^{\sigma\sigma}$ vs pump strength, and then the polarization degree $P = (n_{\text{tot}}^x - n_{\text{tot}}^y)/(n_{\text{tot}}^x + n_{\text{tot}}^y)$, which varies between $P = 1$ for a fully x polarized condensate, to $P = 0$ for a fully unpolarized state, to $P = -1$ for fully y polarized. As anticipated above, for a fully polarized pump, the degree of polarization increases significantly at the same point that the total photon population changes from increasing linearly with pump to superlinearly, i.e. at the point where macroscopic occupation of a single mode, and thus stimulated emission sets in.

The middle panel of Fig. 3 shows the corresponding behavior of three of the angular moments of the molecular distribution, $N_{0,0}$, $N_{2,0}$ and $N_{2,2} = N_{2,-2}$. The lowest order component corresponds to an overall scale of the molecular excitation, and as one may expect, it increases with pumping below threshold, and then saturates at threshold. More notably, for the components with $l = 2$, these decrease above threshold. When both polarization components are above threshold, the chemical potential of light, μ must be locked at the frequency of the lowest cavity mode, i.e. $\mu = \delta_0$. If the molecular distribution were to come into equilibrium with this, then one would require an equilibrated distribution $N_\gamma(\theta, \phi) = [e^{-\beta\mu} + 1]^{-1}$ independent of angle, which

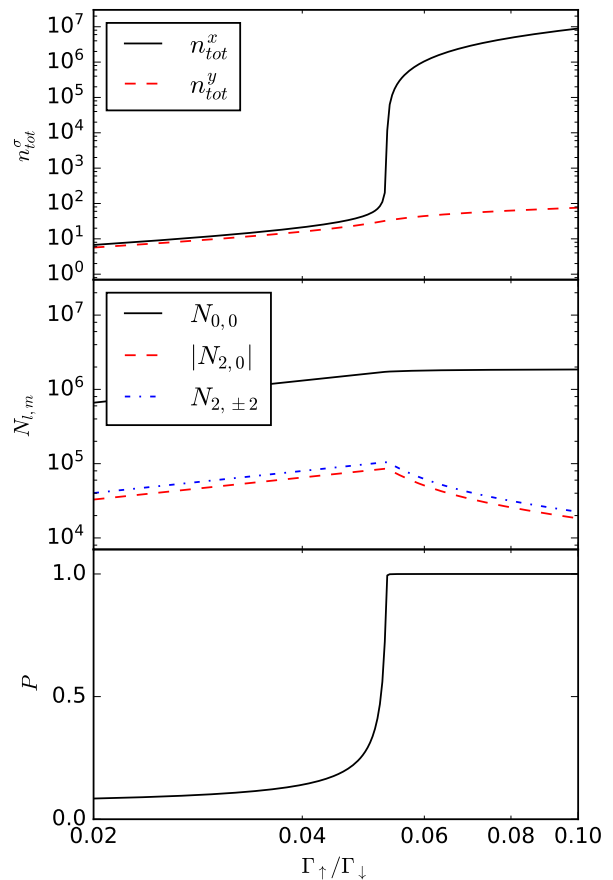


FIG. 3. Total polarization as a function of dimensionless pump strength $\Gamma_\uparrow/\Gamma_\downarrow$ for a fully x polarized pump. The top panel shows total intensity $n_{\text{tot}}^\sigma = \sum_m n_m^{\sigma\sigma}$ as a function of pump strength for $\sigma = x, y$. The middle panel shows the population of molecules in each of the lowest order spherical harmonics. Bottom panel shows the corresponding value of $P = (n_{\text{tot}}^x - n_{\text{tot}}^y)/(n_{\text{tot}}^x + n_{\text{tot}}^y)$. We see that at the condensation threshold, the degree of polarization increases significantly.

would imply $N_{l,m} \rightarrow 0$ for all $l, m > 0$. This behavior is the polarization equivalent of gain saturation leading to a spatially flat excitation profile in an inhomogeneous pump spot [22].

C. Dependence on cavity loss rate

In Figure 3, over the range of pumping shown, only the majority polarization component acquires a macroscopic population. However, this is not always the case. For comparison, Fig. 4 shows the same quantities as Fig. 3 but for a smaller cavity loss rate κ . In this case, one sees that both components reach threshold (both components show a nonlinear increase of population at a critical pumping strength). In contrast, if we increase the cavity loss rate, the population of the minority component is reduced. Multiple modes reaching threshold is

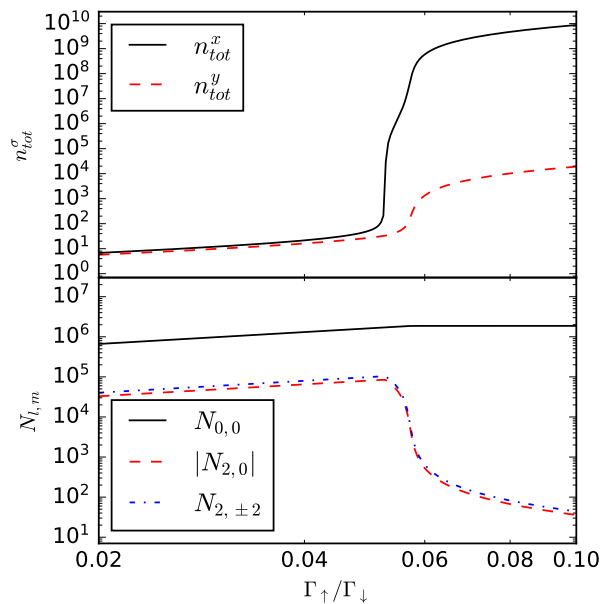


FIG. 4. Total intensity of each polarization vs dimensionless pump power as in Fig. 3, but for a smaller loss rate, $\kappa = 0.5$ MHz. All other parameters as in Fig. 3. With a smaller value of κ , both polarizations go above threshold.

not inherently surprising: multimode behavior has been predicted [22] and observed [23] in the dye-cavity system due to spatial hole burning. In that case, spatial hole burning allows non-degenerate modes with different transverse profiles to reach threshold at a higher pump power than the first lasing mode. Since the two different polarization states are degenerate, the bare emission rates into these modes are equal, and so both modes can in principle reach threshold at the same power.

The above discussion might suggest that in a perfect cavity, i.e. in the limit of vanishing photon loss, polarizations would vanish. However, finite polarization can remain in this limit, despite the fact that the two polarizations are degenerate in energy. To see this, we may consider Eq. (8), from which we see that the steady state photon distribution must obey:

$$\frac{n_m^{xx,yy} + 1}{n_m^{xx,yy}} = \frac{\Gamma(\delta_m)}{\Gamma(-\delta_m)} \frac{N - N^{xx,yy}}{N^{xx,yy}} \quad (12)$$

where we have denoted $N^{xx,yy} = N_{0,0} - N_{2,0}/\sqrt{5} \pm \sqrt{\frac{3}{10}}(N_{2,2} + N_{2,-2})$. Using the Kennard-Stepanov relation between $\Gamma(\pm\delta_m)$, this expression clearly leads to a Bose-Einstein distribution $n_m^{xx,yy} = [\zeta_{xx,yy}^{-1} e^{\beta\delta_m} - 1]^{-1}$ where the fugacity $\zeta_{xx,yy}$ is given by $\zeta_{xx,yy} = N^{xx,yy}/(N - N^{xx,yy})$. In general, $N^{xx} \neq N^{yy}$ (as long as $N_{2,\pm 2}$ is strictly non-zero), so these fugacities differ. Since the fugacity of the majority component must be close to $\zeta = e^{\beta\delta_0}$, a very small difference in N^{xx} , N^{yy} is sufficient to sustain a large difference in photon population. Indeed, as seen in the central panel of Fig. 3 the

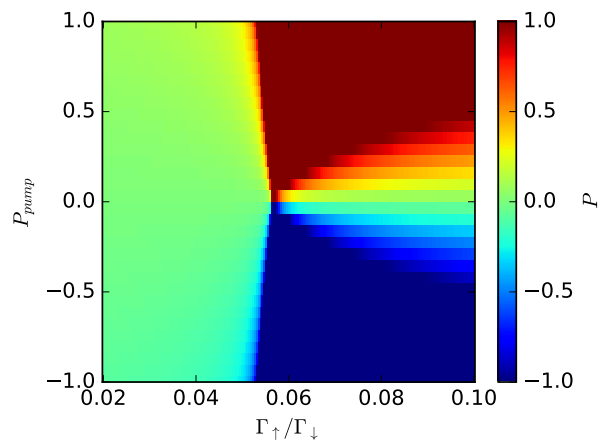


FIG. 5. Colormap of polarization degree, P as defined in Fig. 3, as a function of dimensionless pump power (horizontal axis) and polarization degree of pump (vertical axis).

value of $N_{2,\pm 2}$ actually approaches zero above threshold, but the residual non-zero value leads to a finite polarization of the light.

D. Dependence on input polarization

Having identified a single parameter P that defines the polarization state, we use this in Fig. 5 to show how the evolution of polarization degree with pump power varies according to pump polarization. Below threshold, as noted above, the state is very weakly polarized, and only weakly dependent on the polarization degree of the light. Just above threshold, the majority photon polarization grows faster than the minority, and so there is almost complete polarization in this limit, with the output polarization switching between $+1$ and -1 depending on the sign of the input polarization. The threshold power depends on the polarization degree. This is expected, as a high polarization degree means that more of the input power can go into feeding the majority polarization component, and so that component reaches threshold sooner. Further above threshold (i.e. at the largest values of Γ_{\uparrow} shown in Fig. 5), the minority photon polarization also becomes large, so the polarization degree reduces, leading to a more gradual dependence on the input polarization. This is particularly noticeable for smaller input polarization degree.

E. Effect of diffusion constant

As noted above, the difference in polarization degree from below to above threshold originates from the competition between the timescale for diffusion, and the timescale for (stimulated) fluorescence from the dye molecules. Figure 6 shows the effect of the diffusion con-

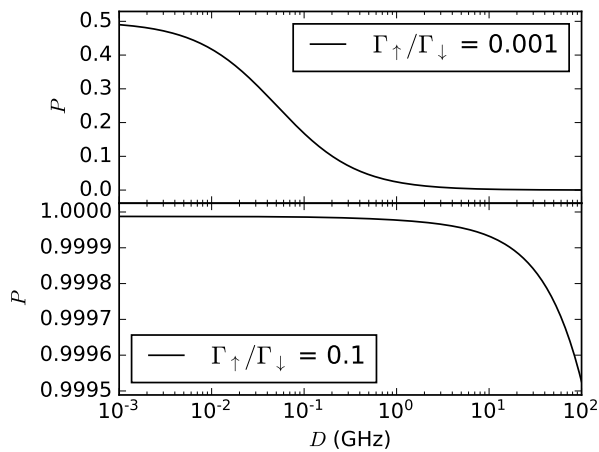


FIG. 6. Polarization degree, P , as defined in Fig. 3 as a function of angular diffusion constant of molecules, D for a pump power below threshold (top) and above threshold (bottom).

stant on this. The behavior is shown both below and above threshold, considering a fully x polarized pump in both cases.

Well below threshold, there is a gradual increase of the polarization degree as the diffusion constant reduces. When the diffusion constant is zero, there is no molecular rotation; despite this, the system does not become fully polarized, but reaches a value $P = 0.5$. This is because, as discussed above, most molecules can couple both to x and y polarized light. This means that a purely x polarized pump excites molecules that can subsequently emit into both x and y polarized modes.

We can understand the limiting value $P = 0.5$ by considering the behavior of Eq. (7) for weak pumping and zero diffusion. In the weak pumping limit, the cavity population is small so all cavity mediated terms can be neglected. Considering a fully polarized pump ($\chi = 0$), the steady state of this equation becomes:

$$\Gamma_{\downarrow} N_{\uparrow}(\theta, \phi) = \Gamma_{\uparrow} \sin^2(\theta) \cos^2(\phi) [N - N_{\uparrow}(\theta, \phi)].$$

Then if $\Gamma_{\uparrow} \ll \Gamma_{\downarrow}$, this equation implies that $N_{\uparrow}(\theta, \phi) \propto \sin^2(\theta) \cos^2(\phi)$. The polarization degree of light then follows from inserting this form into the integrals in Eq. (4)-(5). This gives the ratio of $n^{xx} : n^{yy}$ in proportion to the overlaps $\int d\phi \cos^2 \phi \cos^2 \phi : \int d\phi \cos^2 \phi \sin^2 \phi$, which produces a ratio 3 : 1, giving $P = 0.5$. From this derivation, it is clear that this result only holds in the limit of very weak pumping. For stronger pumping, the cavity modes become populated. This means that there can be stimulated emission (even below threshold), which favors the majority component, increasing P . Indeed, at large enough pumping, condensation occurs leading to $P \rightarrow 1$, as seen in the bottom panel of Fig. 6.

It is worth discussing why it is physically the case that molecules can couple the two orthogonal polarization modes. This feature (clearly present in the equations) originates from the fact that we assume no intra-

molecular coherence exists, only incoherent absorption and emission by molecules. If the molecules were allowed to retain coherence, emission by molecules at different angles could lead to destructive interference. In such a case, an x polarized pump would lead to a pattern of coherence such that y polarized emission canceled, while x polarized emission was reinforced. The rapid dephasing of the molecules in solution prevents the destructive interference, and so leads instead to the limiting value $P = 0.5$.

IV. CONCLUSIONS

In conclusion, we have developed a model to describe the polarization states of a BEC of photons in a dye-filled cavity. This model extends our previous work [9, 16], accounting for the polarization states of light, and the effects of angular diffusion of the dye on the polarization state.

We find distinct behavior above and below threshold. Below threshold, photon emission is slow, and so rotational diffusion of the molecules washes out the pump polarization. Above threshold, fast stimulated emission leads to a greater dependence on pump polarization state. We assume coherence of the molecules is rapidly lost due to collisions between dye and solvent molecules. As a result, a fully polarized pump can always produce light with the opposite polarization, even without diffusion. This is because most molecules can (incoherently) absorb and emit both polarizations of light, and without coherence, no cancellations can occur. Thus, for a fully polarized pump far below threshold, the output polarization varies between $P = 0$ (when diffusion is very fast) and $P = 0.5$ when diffusion vanishes, and molecules fail to rotate. In contrast, above threshold, stimulated emission allows the majority polarization to dominate, leading to nearly complete polarization, $P \rightarrow 1$.

As the photon BEC is a driven dissipative system, it is not surprising that the pump polarization can have an effect on the output states. However, it is notable that our model predicts this dependence survives even in the limit of vanishing cavity loss, $\kappa \rightarrow 0$. This means there is an absence of thermalization of polarization. This is in contrast to thermalization between different spatial modes of the cavity — here, the $\kappa \rightarrow 0$ limit of our model is known to lead to a perfectly thermal distribution [16]. The difference between the thermalization of spatial modes, and absence of thermalization for polarization modes can be traced back to the nature of how the molecules act as a reservoir. For large pumping spots [22], all spatial modes couple to exactly the same set of molecules as a reservoir. In contrast, the two polarizations of light couple differently to molecules at different angles, meaning that full equilibration need not occur.

The results we present here provide not only a way to model the polarization dynamics of a photon condensate, but also provide a clear understanding of why the

model behaves as it does. Our work was focused on the current experiments where the medium in the cavity is not significantly birefringent. An interesting extension of our work would be to consider birefringent materials, where energetics could favor one polarization state, and may then compete with that favored by pumping. The research data supporting this publication can be found at doi: 10.17630/e9a4fda9-3f3c-4f23-a6fc-227de27c9851.

ACKNOWLEDGMENTS

We acknowledge helpful discussions with R. Nyman and K. E. Ballantine. RIM acknowledges support from the “Laidlaw Research Internship” scheme at the University of St Andrews. PK acknowledges support from EPSRC (EP/M010910/1). JK acknowledges support from EPSRC programs “TOPNES” (EP/I031014/1) and “Hybrid polaritonics” (EP/M025330/1).

-
- [1] J. Klaers, F. Vewinger, and M. Weitz, *Nat. Phys.* **6**, 512 (2010).
- [2] J. Klaers, J. Schmitt, F. Vewinger, and M. Weitz, *Nature* **468**, 545 (2010).
- [3] E. H. Kennard, *Phys. Rev.* **11**, 29 (1918).
- [4] E. H. Kennard, *Phys. Rev.* **28**, 672 (1926).
- [5] B. I. Stepanov, *Dokl. Akad. Nauk SSR* **112**, 839 (1957).
- [6] J. Klaers, J. Schmitt, T. Damm, F. Vewinger, and M. Weitz, *Phys. Rev. Lett.* **108**, 160403 (2012).
- [7] D. N. Sob'yanin, *Phys. Rev. E* **85**, 061120 (2012).
- [8] D. W. Snoke and S. M. Girvin, *J. Low Temp. Phys.* **171**, 1 (2013).
- [9] P. Kirton and J. Keeling, *Phys. Rev. Lett.* **111**, 100404 (2013).
- [10] A. Kruchkov, *Phys. Rev. A* **89**, 033862 (2014).
- [11] E. C. I. van der Wurff, A.-W. de Leeuw, R. A. Duine, and H. T. C. Stoof, *Phys. Rev. Lett.* **113**, 135301 (2014).
- [12] A.-W. de Leeuw, H. T. C. Stoof, and R. A. Duine, *Phys. Rev. A* **89**, 053627 (2014).
- [13] A. Chiochetta and I. Carusotto, *Phys. Rev. A* **90**, 023633 (2014).
- [14] R. A. Nyman and M. H. Szymańska, *Phys. Rev. A* **89**, 033844 (2014).
- [15] E. Sela, A. Rosch, and V. Fleurov, *Phys. Rev. A* **89**, 043844 (2014).
- [16] P. Kirton and J. Keeling, *Phys. Rev. A* **91**, 033826 (2015).
- [17] A.-W. de Leeuw, E. C. I. van der Wurff, R. A. Duine, and H. T. C. Stoof, *Phys. Rev. A* **90**, 043627 (2014).
- [18] J. Schmitt, T. Damm, D. Dung, F. Vewinger, J. Klaers, and M. Weitz, *Phys. Rev. A* **92**, 011602 (2015).
- [19] J. Schmitt, T. Damm, D. Dung, F. Vewinger, J. Klaers, and M. Weitz, *Phys. Rev. Lett.* **112**, 030401 (2014).
- [20] A. Chiochetta, A. Gambassi, and I. Carusotto, in *Universal Themes of Bose-Einstein Condensation*, edited by N. P. Proukakis, D. W. Snoke, and P. B. Littlewood (Cambridge University Press, Cambridge, 2017) 1503.02816.
- [21] J. Marelic and R. A. Nyman, *Phys. Rev. A* **91**, 033813 (2015).
- [22] J. Keeling and P. Kirton, *Phys. Rev. A* **93**, 013829 (2016).
- [23] J. Marelic, L. Zajiczek, H. Hesten, K. Leung, E. Ong, F. Mintert, and R. Nyman, *New Journal of Physics* **18**, 103012 (2016).
- [24] J. Marelic, B. T. Walker, and R. A. Nyman, *Phys. Rev. A* **94**, 063812 (2016).
- [25] J. Klaers and M. Weitz, “Bose-Einstein condensation of photons and grand-canonical condensate fluctuations,” (2016), preprint, 1611.10286.
- [26] H. J. Hesten, R. A. Nyman, and F. Mintert, “Decondensation in non-equilibrium photonic condensates: when less is more,” (2017), preprint, 1705.02173.
- [27] R. A. Nyman and B. T. Walker, “Bose-Einstein condensation of photons from the thermodynamic limit to small photon numbers,” (2017), preprint, 1706.09645.
- [28] H. Jagers, *Polarization of a Photon Bose-Einstein Condensate*, B.S. Thesis, Utrecht University (2016).
- [29] R. Nyman, Private Communication (2016).
- [30] J. Stenger, S. Inouye, D. Stamper-Kurn, H.-J. Miesner, A. Chikkatur, and W. Ketterle, *Nature* **396**, 345 (1998).
- [31] L. Sadler, J. Higbie, S. Leslie, M. Vengalattore, and D. Stamper-Kurn, *Nature* **443**, 312 (2006).
- [32] D. M. Stamper-Kurn and M. Ueda, *Rev. Mod. Phys.* **85**, 1191 (2013).
- [33] M. Salomaa and G. Volovik, *Rev. Mod. Phys.* **59**, 533 (1987).
- [34] A. J. Leggett, *Quantum Liquids: Bose Condensation and Cooper Pairing in Condensed-Matter Systems* (Oxford University Press, 2006).
- [35] I. A. Shelykh, A. V. Kavokin, Y. G. Rubo, T. C. H. Liew, and G. Malpuech, *Semiconductor Science and Technology* **25**, 013001 (2010).
- [36] A. V. Larionov, V. D. Kulakovskii, S. Höfling, C. Schneider, L. Worschech, and A. Forchel, *Phys. Rev. Lett.* **105**, 256401 (2010).
- [37] L. Klopotoski, M. D. Martín, A. Amo, L. Viña, I. Shelykh, M. Glazov, G. Malpuech, A. Kavokin, and R. André, *Solid State Commun.* **139**, 511 (2006).
- [38] J. Kasprzak, R. André, L. S. Dang, I. A. Shelykh, A. V. Kavokin, Y. G. Rubo, K. V. Kavokin, and G. Malpuech, *Phys. Rev. B* **75**, 045326 (2007).
- [39] F. P. Laussy, I. A. Shelykh, G. Malpuech, and A. Kavokin, *Phys. Rev. B* **73**, 035315 (2006).
- [40] D. D. Solnyshkov, I. A. Shelykh, and G. Malpuech, *Phys. Rev. B* **80**, 165329 (2009).
- [41] R. A. Nyman, “Absorption and Fluorescence spectra of Rhodamine 6G,” (2017).
- [42] A. Von Jena and H. Lessing, *Chemical Physics* **40**, 245 (1979).